Wheaton Journal of
Neurobiology Research

Issue 12, Fall 2019:

“Experiments modeling Alzheimer’s, concussion, vaping, and stress in culture"

R.L. Morris Ph.D., Editor. Wheaton College, Norton, Massachusetts.

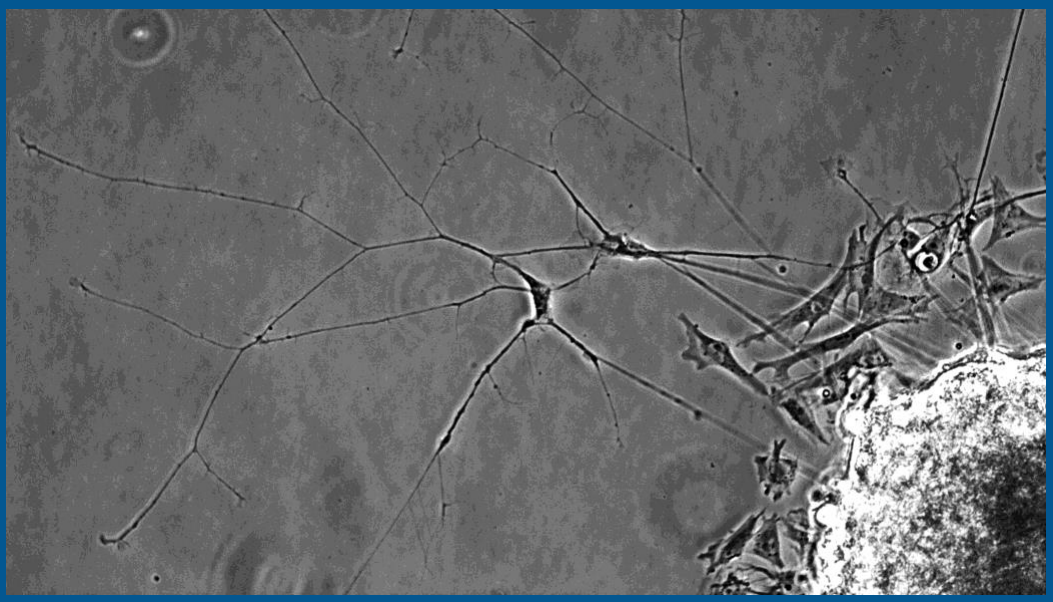

Evidence that varicosity prevalence increases with distance from applied mechanical force injury in *Gallus gallus* neurons

Morgan M. Karnes

BIO 324 / Neurobiology
Final Research Paper
4 December 2019

Evidence that varicosity prevalence increases with distance from applied mechanical force injury in *Gallus gallus* neurons

Morgan M. Karnes
Final Research Paper written for
Wheaton Journal of Neurobiology Research
BIO 324 / Neurobiology
Wheaton College, Norton Massachusetts
4 December 2019

Introduction

A traumatic brain injury (TBI) is a common injury caused by a blow to the head and alters normal brain functioning for an extended period of time. A concussion is considered a mild traumatic brain injury (mTBI). There are over a million concussions diagnosed in the United States every year (Langlois, Rutland-Brown, & Wald, 2006). In general, a concussion occurs when the head undergoes non-penetrating force accompanied by a quick response in movement: acceleration, deceleration or specific rotation of the head (Bigler, 2019). The brain is suspended in cerebral fluid but is secured and protected by the skull. When there is a physical impact to the head with sudden directional movement, the brain will move through the fluid hitting the inside of the skull (Dashnaw, Petraglia, & Bailes, 2012). This physical force results in stress to the axons, concentrated towards the center of the brain mass. These axons compose the brain's white matter. The gray matter is composed of the area surrounding the white matter on the outer edges of the brain, which is enriched in cell bodies. With many mTBI and other severe cases, axonal transport is interrupted due to blebs that occur as the microfilaments in the axon lose their structure (Dashnaw et al., 2012).

There is evidence that the region of injury matters when it comes to effects on the brain and neurons (Conti, Raghupathi, Trojanowski, & McIntosh, 1998). It is also known that the biomechanics of a head injury in terms of how the head and brain are shifted– acceleration, deceleration, or rotation, for example– influences the subsequent response in the gray matter and corresponding response of the axons in the white matter (Raghupathi, 2004). These findings suggest that the gray matter containing the cell bodies respond in a different way than the axons of the white matter. Specifically, it has been found that morphological and functional damage such as alterations in biochemical and physiological pathways occurs in the white matter, leading to diffuse axonal injury (Alder, Fujioka, Lifshitz, Crockett, & Thakker-Varia, 2011). There is evidence that with a diffuse axonal injury, structural microtubules in axons can be physically broken. This leads to bulbous swelling or varicosity formation and interrupts intracellular axonal transport (Tang-Schomer, Johnson, Baas, Stewart, & Smith, 2012). However, many mechanisms that initiate these kinds of changes are not fully understood.

In this study, a mechanical force apparatus was constructed to expel liquid simulating a mTBI, with alterations from the model of a fluid percussion injury (Carbonell & Grady, 1999). The liquid loaded in the mechanical force apparatus was released onto a designated ganglion of peripheral neurons from *Gallus gallus*, the domesticated chicken, in a culture dish. A close and

far region of the targeted ganglion were defined and analyzed for varicosity density. This study tested the hypothesis that there would be a greater number of varicosities per axon in the region closest to where applied mechanical force was released as compared to regions farther away from the impact center. This study was done in collaboration with Laura Scheidemantel, Lilly Callahan, and Emma Paolella.

Materials and Methods

Primary Culture and Dissection of embryonic Gallus gallus neurons

The procedure for culture conditions and embryonic dissection of Gallus gallus neurons was obtained from a published procedure (Morris, 2017). The coverslips on which the cultures were plated were cleaned following the noted procedure by Morris. The embryos were dissected 10 days following fertilization. Once the dorsal root ganglion and sympathetic nervous chains were isolated and the cultures were plated, the dishes were stored in an incubator at 37°C overnight. Dorsal root ganglion isolation was performed by Robert L. Morris of the Biology department at Wheaton College in Norton, Massachusetts.

Construction of Mechanical Force Apparatus

Methods development and construction of mechanical force apparatus were derived with adaptation from "Polarity of varicosity initiation in central neuron mechanosensation," (Gu et al., 2017). An open, gas-fueled flame was used to constrict a 9-inch plugged pasteur pipette by rolling and pulling the end while warm to a desired inner diameter of 50 μm. A Nikon SMZ800N dissection scope was set up with a 100 μm-10 μm measuring slide to confirm the diameters of the pipettes. A diamond-studded pencil was used to scratch off the thicker end of the pipette for the desired diameter. Seven total pipettes were obtained. The pipette tips were later broken as the small diameter did not allow liquid to flow through. As a result, a pipette with an inner diameter of approximately 300 μm or 0.3 mm at the end was used.

Two sizes of plastic tubing were obtained: a 4 mm diameter tube and a 6 mm diameter tube. The 4 mm tubing was cut into a singular one-inch length and then placed just inside the 6 mm tubing at one end. This modified end was attached to a 20 mL syringe to hold a tight seal between the syringe and tubing. The 6 mm tubing was cut at approximately 25 cm length, and also attached to the constricted pipette. The tubing, syringe, and pipette did not need to be autoclaved since the samples were discarded within an hour of treatment and were not cultured for any prolonged period after treatment.

The testing station was constructed by securing two magnetic base ring stands to a metal table. Next, the glass pipette was clamped into a three-pronged clamp that was attached to a micromanipulator, which had been secured to one of the magnetic ring stands. The 20 mL syringe at the end of the tubing was attached to prongs on the second magnetic ring stand. The magnetic table, or sheet, was placed directly next to the dissecting scope to be used for impact monitoring. Since the cells of interest were not to be incubated for any period of time over an hour or two, the tubing, syringe and pipette did not need to be autoclaved for sterility.

Performing the Mechanical Force Injury

A dish of cultured plated ganglia in a 35 mm petri dish was used one day following neuron dissection. This dish was imaged using a Nikon Eclipse TS100 inverted microscope to identify regions with many ganglia and a high density of axons present at either 10X or 40X objective magnification. This region of interest was marked with a permanent marker on the

plastic petri dish in two places, forming coordinates of the particular region to be hit. Images were taken of the marked region for control purposes to examine the ganglia before treatment. With the tubing disconnected from the pipette, approximately 20 mL of Hank's Balanced Salt Solution (HBSS) was poured into the syringe. The tubing was held up in the air to prevent spillage and kept at an even height with the level of the liquid in the syringe so as to balance out the pressure differential. Once the HBSS was set, the syringe cap was placed on the syringe to block the system and any spontaneous liquid flow. The pipette, still disconnected from the tubing, was secured in the micromanipulator.

An extra 35 mm petri dish with an empty coverslip was placed under the dissecting scope. The pipette was positioned over the dish and then slowly lowered to the top of the coverslip. The coordinates of each of the three axes from the micromanipulator were recorded in this position. The pipette was then raised as close to 0.4 mm above the coverslip as possible, as originally demonstrated by Gu et al., (2017). This second vertical coordinate was recorded for replication. The empty petri dish was then replaced by the petri dish with the sample on the dissecting scope. Using the dissecting scope, the region of interest was located with the marks on the dish. With the pipette upside-down, the tubing was then connected to the pipette. The HBSS filled the length of the pipette and air bubbles were removed. Once the dissecting scope was in focus on the interest region, the pipette was then secured in the micromanipulator and quickly moved to the previously found position using the recorded coordinates.

The height of the syringe was set so that the distance between the height of the liquid in the syringe and the tip of the pipette was 190 mm. This was done so that the pressure of the liquid being expelled onto the cells was 190 mm H_2O, as demonstrated by Gu et al., (2017). Once the ganglia of interest were in focus and the tubing and pipette were set, the syringe cap was removed so that the liquid would begin to flow out. After liquid flowed out for approximately ten seconds, the pipette was angled up and the syringe was lowered to stop the liquid flow and decrease the pressure. Then the pipette was raised up and taken out of the clamp so that the petri dish could be removed. The petri dish was then carefully transferred back to the inverted scope in order to obtain images at a higher magnification than the dissecting scope would allow. The above procedure was executed on three separate instances.

Imaging Injured Neurons

The sample dish was transferred to an inverted microscope to image the ganglion that was injured. The coordinates marking the location of the ganglion were used to locate the cells of interest under the microscope. A Nikon Eclipse TS100 inverted microscope was connected to an iMac desktop computer running MacOS High Sierra 10.13.6 software and the imaging application SPOT version 5.2. This program allowed the image viewed in the binoculars of the microscope to be seen on the computer with options to adjust contrast and white balance. Transmitted light images were taken centered at the ganglion. More images were also taken when the ganglion was in the corner of the image, allowing more axons and an increased diameter to be in view. Images in this orientation were taken circularly all around the ganglion. Images were either taken at a 10X objective magnification or 40X objective magnification.

Data Analysis

Data quantification was performed using the application ImageJ. Images of the injured ganglia were opened using this application. An image of the 100 μm-10 μm measuring slide was captured on the same Nikon Eclipse TS100 inverted microscope used to view and capture the

ganglia. The image of the ruler slide was taken at 10X objective magnification. This image was then opened in ImageJ. A line segment was drawn from one mark on the ruler to another for a known distance of 400 μm. This line was measured in pixels by one of the "Analyze" options in the menu bar. The scale was changed to micrometers by using another one of the "Analyze" options. The known distance of the line in micrometers was entered and the scale was set to be applied globally. The "Set Measurements" settings were manipulated to ensure the lines drawn for measurements would remain on the image collectively. The following options were selected for this: "Area," "Min and max gray value," "Center of mass," "Area Fraction," "Mean gray value," "Area fraction," and "Add to overlay." A circle was drawn on the first image using the Oval/Ellipses tool, in which the edge of the circle was placed at the center of the impact point and the diameter of the circle was 300 μm. From there, a line segment was drawn from the center impact point, through the center of the close circle and an additional 150 μm outwards. This marked the outer edge of the far region, again indicated by a 300 μm diameter circle.

The close and far circles were analyzed for varicosities present along all axons inside each region. Axons were defined as a uniform-caliber extension of the cell, and a varicosity was defined as a region along the axon which had a 150% larger width than a nearby region of the same axon. Axons were measured using the same "Analyze" tool as before. Any swelling along an axon would be measured with the line segment tool and compared numerically to the width of the adjacent region of the same axon. If the ratio of the larger measurement to the smaller width was greater than 1.5, the location and ratio were recorded. All axons present in the circular regions were included and measured. This same technique was used on one other image from another trial. The pixel to μm scale had to be multiplied by 4 and changed manually for the second image because it was taken at 40X objective magnification.

The cumulative measurement table was saved and then imported into Microsoft Excel. The data was then manipulated into a table containing data for each axon length and the count of varicosities found along that specific axon for all of the close data and the far data. After that, the ratio of varicosities per axon length was calculated and multiplied by 100 to get the varicosity density per 100 μm axon length. The standard deviations for the close data set and the far data set were also calculated in Excel. Regions chosen for imaging were selected based on presence of axons to measure. In an attempt to limit bias in the data set, all axons present in each of the designated regions, close and far from impact, were included in the data measurement.

Results

The hypothesis that the region nearest a ganglion injured by applied mechanical force has a higher density of varicosities than a region farther from the impact center was tested and quantified using images of the targeted ganglion after injury. The ganglia that were imaged prior to any treatment displayed clean, smooth axons (Figure 1). The ganglia that were imaged after having been injured by applied mechanical force showed more bends and swelling of the axons, suggestive of varicosities (Figure 2). These images, particularly Figure 2, indicate the successful application of mechanical force to the ganglion using the methods developed in this study. It should be noted that the two images shown are not identical regions, but different ganglia from the same dish. Figure 1 shows a ganglion that was not targeted, while Figure 2 shows the targeted ganglion from this specific trial. Varicosity density was scaled to obtain the number of varicosities per 100 μm of axon length. After analysis, the designated far region was found to have a higher density of varicosities than the region closer to the impact epicenter (Figure 3). The standard deviation for both of these sets was high.

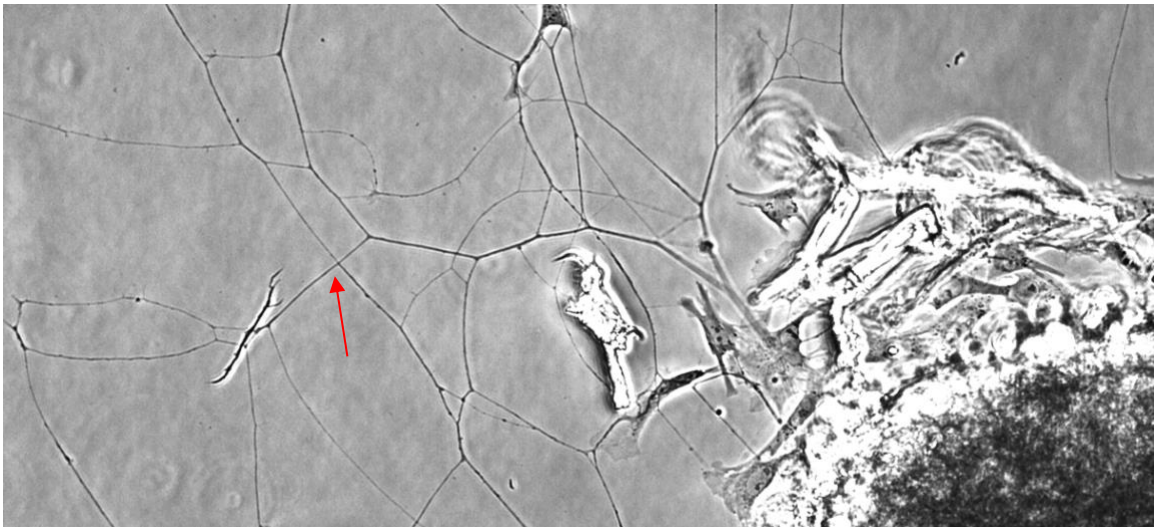

Figure 1: A ganglion and axons before treatment of applied mechanical force. This transmitted light image shows a ganglion that had not experienced applied mechanical force. It shows a junction of two axons extending from the ganglion with an arrow indicating that they are smooth and thin. Notice the absence of swelling along the axon lengths, suggesting minimal to no varicosities present. The image was taken at 40X objective magnification, and brightness and contrast were adjusted in Photoshop. The horizontal width of the image is 218.6 μm.

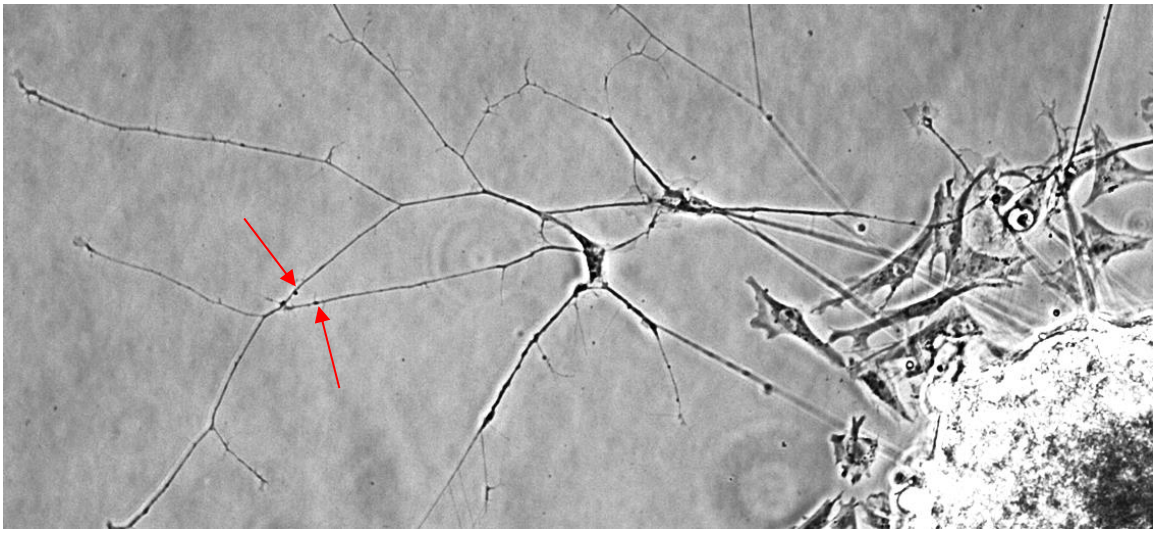

Figure 2: A ganglion and axons after applied mechanical force at its center. This transmitted light image shows the ganglion that experienced applied mechanical force. It includes a portion of the targeted ganglion, glial cells surrounding this and axons extending from the ganglion. The red arrows indicate swelling of axons in two different places, appearing as small, round dots. Notice that the axons appear contorted, and they are not as linear as before treatment (Figure 1). This image was taken at 40X objective magnification, and brightness and contrast were adjusted in Photoshop. The horizontal width of the image is 217.2 μm.

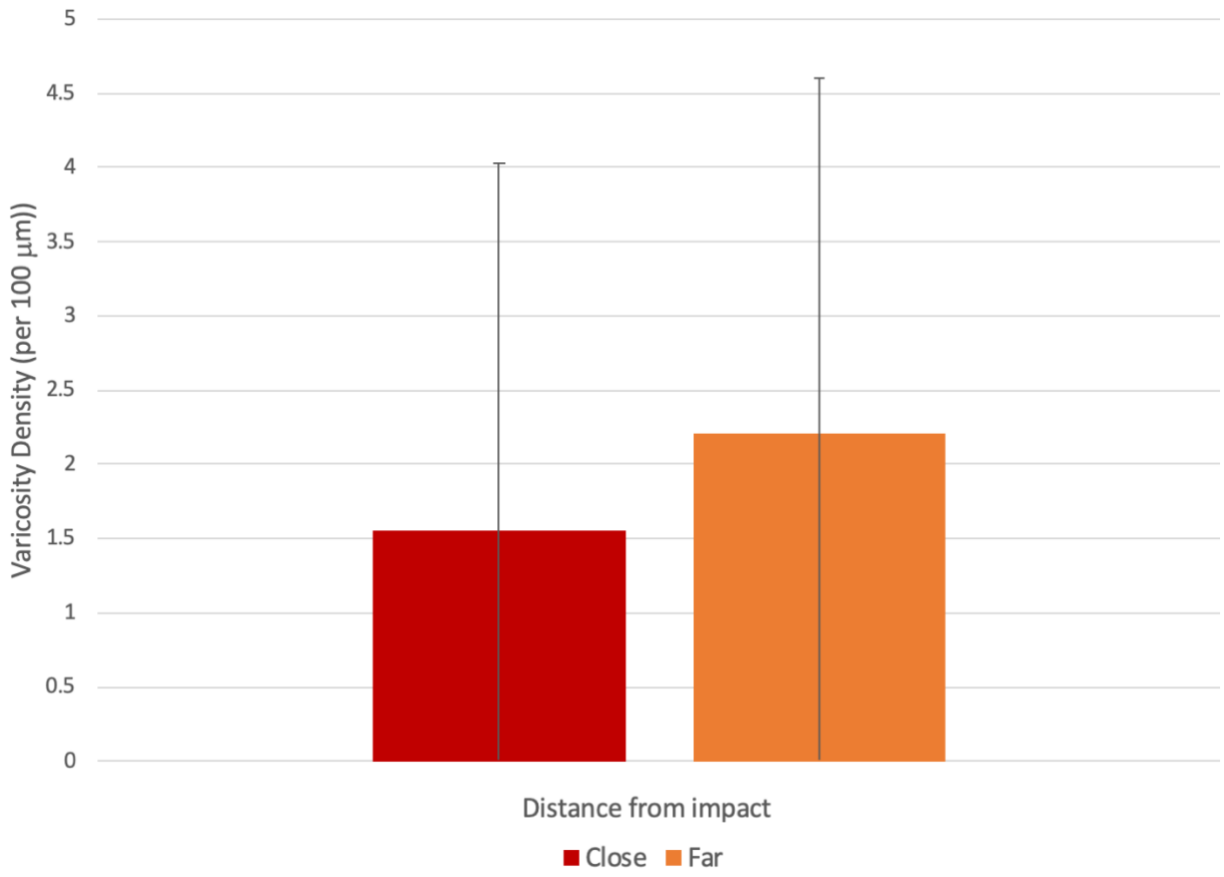

Figure 3: The varicosity density in close and far regions from applied mechanical force. This graph shows the average varicosity density, measured by the number of varicosities per 100 µm of axon length, in close and far regions from applied mechanical force. The close region, indicated in red, had a lower average varicosity density than the far region, indicated in orange. In the close region, a total of 43 axons were measured for length and surveyed for varicosities derived from two images, each from separate trials. In the far region, a total of 8 axons were measured for length and surveyed for varicosities derived from the same two images as the close regions from two separate trials. Notice the high standard deviation values for each data set.

Discussion

Understanding more about the mechanisms of mTBI and differences in subsequent axon damage like varicosities can allow for further studies and the development of treatments for this widespread injury. The results of this study do not support the stated hypothesis that there would be a greater varicosity density in the region closest to where mechanical force was applied as compared to regions farther away from the impact point. Since there is a higher varicosity density in the far region, it might be conjectured that perhaps the axons of the white matter are more susceptible to injury. In addition, lower varicosity density in the gray matter, which is enriched by the neuron cell bodies and regionally closer to the impact, might be evidence that there is a difference in physical or mechanical properties between gray and white matter. Previous studies have found that gray and white matter have distinct stiffness characteristics, which could possibly affect microtubule stability (Budday et al., 2015). While this study does not

contain significant data, there were no explicit findings to contradict the analyzed trend of the data. Possible sources of variability in the study include an inconsistency from the mechanical force apparatus in regard to identical volumes and pressures during each trial.

The structural and physiological differences in composition between the gray matter and white matter could have been a potential factor in the prevalence of varicosities per region. One possible explanation behind the noticeable axon damage might be due to a loss of control of calcium ion reserves (Stys, 1998). In a similar study to this one, neurons were analyzed using proton magnetic resonance spectroscopy to differentiate select chemicals in the brain after a mTBI (Gasparovic et al., 2009). They found that the levels of glutamate, one of the brain's major neurotransmitters, and creatine-phosphocreatine had deviated from equilibrium concentrations after a mTBI. Further, these changes in concentrations were different in the white matter versus the gray matter, which indicates a difference in metabolic processes in the two types of matter (Gasparovic et al., 2009). It might be possible that structural damage from a mTBI could cause detriment to the metabolism in gray and white matter, especially since such injury restricts axonal transport through microtubule disruption (Tang-Schomer et al., 2012; Tang-Schomer, Patel, Baas, & Smith, 2010).

The results of studies such as this one are crucial in developing more precise treatment for a mTBI. By understanding the primary mechanisms of neuronal processes after a mTBI, targeted treatments can be developed to prevent or lessen the negative cognitive effects of this injury. Head injuries, specifically a mTBI, are very common but remain without any comprehensive Federal Drug Administration approved treatments (Arciniegas, Anderson, Topkoff, & McAllister, 2005). There is still a gap in extensive knowledge of metabolic and biochemical pathways in gray matter and white matter in the brain during and after a mTBI. Future studies should investigate the change in enzyme abundance and concentration between gray and white matter after a mTBI. Specifically, enzymes which are involved in microtubule degeneration and those crucial to axonal transport should be investigated.

References

Alder, J., Fujioka, W., Lifshitz, J., Crockett, D. P., & Thakker-Varia, S. (2011). Lateral Fluid Percussion: Model of Traumatic Brain Injury in Mice. *Journal of Visualized Experiments*, (54). https://doi.org/10.3791/3063

Arciniegas, D. B., Anderson, C. A., Topkoff, J., & McAllister, T. W. (2005). Mild traumatic brain injury: a neuropsychiatric approach to diagnosis, evaluation, and treatment. *Neuropsychiatric Disease and Treatment*, *1*(4), 311–327. Retrieved from http://www.ncbi.nlm.nih.gov/pubmed/18568112%0Ahttp://www.pubmedcentral.nih.gov/articlerender.fcgi?artid=PMC2424119

Bigler, E. D. (2019). *Neuropsychology and clinical neuroscience of persistent post-concussive syndrome*. https://doi.org/10.1017/S135561770808017X

Budday, S., Nay, R., de Rooij, R., Steinmann, P., Wyrobek, T., Ovaert, T. C., & Kuhl, E. (2015). Mechanical properties of gray and white matter brain tissue by indentation. *Journal of the Mechanical Behavior of Biomedical Materials*, *46*, 318–330. https://doi.org/10.1016/j.jmbbm.2015.02.024

Carbonell, W. S., & Grady, M. S. (1999). Regional and temporal characterization of neuronal, glial, and axonal response after traumatic brain injury in the mouse. *Acta Neuropathologica*, *98*(4), 396–406. https://doi.org/10.1007/s004010051100

Conti, A. C., Raghupathi, R., Trojanowski, J. Q., & McIntosh, T. K. (1998). Experimental brain injury induces regionally distinct apoptosis during the acute and delayed post-traumatic period. *Journal of Neuroscience*, *18*(15), 5663–5672. https://doi.org/10.1523/jneurosci.18-15-05663.1998

Dashnaw, M. L., Petraglia, A. L., & Bailes, J. E. (2012). An overview of the basic science of concussion and subconcussion: where we are and where we are going. *Neurosurgical Focus*, *33*(December), 1–9. https://doi.org/10.3171/2012.10.FOCUS12284

Gasparovic, C., Yeo, R., Mannell, M., Ling, J., Elgie, R., Phillips, J., … Mayer, A. R. (2009). Neurometabolite concentrations in gray and white matter in mild traumatic brain injury: An 1H-magnetic resonance spectroscopy study. *Journal of Neurotrauma*, *26*(10), 1635–1643. https://doi.org/10.1089/neu.2009.0896

Gu, Y., Jukkola, P., Wang, Q., Esparza, T., Zhao, Y., Brody, D., & Gu, C. (2017). Polarity of varicosity initiation in central neuron mechanosensation. *Journal of Cell Biology*, *216*(7), 2179–2199. https://doi.org/10.1083/jcb.201606065

Langlois, J. A., Rutland-Brown, W., & Wald, M. M. (2006). The Epidemiology and Impact of Traumatic Brain Injury A Brief Overview. In *J Head Trauma Rehabil* (Vol. 21). Retrieved from www.headtraumarehab.com

Morris, R. L. (2017). *Primary Culture of Chick Embryonic Peripheral Neurons 1: DISSECTION*. Norton, MA.

Raghupathi, R. (2004). Cell Death Mechanisms Following Traumatic Brain Injury. *Brain Pathology*, *14*(2), 215–222. https://doi.org/10.1111/j.1750-3639.2004.tb00056.x

Stys, P. K. (1998). Anoxic and ischemic injury of myelinated axons in CNS white matter: From mechanistic concepts to therapeutics. *Journal of Cerebral Blood Flow and Metabolism*, Vol. 18, pp. 2–25. https://doi.org/10.1097/00004647-199801000-00002

Tang-Schomer, M. D., Johnson, V. E., Baas, P. W., Stewart, W., & Smith, D. H. (2012). Partial interruption of axonal transport due to microtubule breakage accounts for the formation of periodic varicosities after traumatic axonal injury. *Experimental Neurology*, *233*(1), 364–372. https://doi.org/10.1016/j.expneurol.2011.10.030

Tang-Schomer, M. D., Patel, A. R., Baas, P. W., & Smith, D. H. (2010). Mechanical breaking of microtubules in axons during dynamic stretch injury underlies delayed elasticity, microtubule disassembly, and axon degeneration. *FASEB Journal*, *24*(5), 1401–1410. https://doi.org/10.1096/fj.09-142844

I have abided by the Wheaton College Honor Code in this work.